CrossMark

ORIGINAL

Tools to evaluate seafloor integrity: comparison of multi-device acoustic seafloor classifications for benthic macrofauna-driven patterns in the German Bight, southern North Sea

Peter Holler[1] · Edith Markert[1] · Alexander Bartholomä[1] · Ruggero Capperucci[1] ·
H. Christian Hass[2] · Ingrid Kröncke[1] · Finn Mielck[2] · H. Christian Reimers[3]

Abstract To determine the spatial resolution of sediment properties and benthic macrofauna communities in acoustic backscatter, the suitability of four acoustic seafloor classification devices (single-beam echosounder with RoxAnn and QTC 5.5 seafloor classification system, sidescan sonar with QTC Swathview seafloor classification, and multi-beam echosounder with QTC Swathview seafloor classification) was compared in a study area of approx. 6 km^2 northwest of the island of Helgoland in the German Bight, southern North Sea. This was based on a simple similarity index between simultaneous sidescan sonar, single-beam echosounder and multi-beam echosounder profiling spanning the period 2011–2014. The results show a high similarity between seafloor classifications based on sidescan sonar and RoxAnn single-beam systems, in turn associated with a lower similarity for the multi-beam echosounder system. Analyses of surface sediment samples at 39 locations along four transects (0.1 m^2 Van Veen grab) revealed the presence of sandy mud (southern and western parts), coarse sand, gravel and cobbles. Rock

outcrops were identified in the north-eastern and eastern parts. A typical *Nucula nitidosa–Abra alba* community was found in sandy muds to muddy sands in the northern part, whereas the southern part is characterised by widespread occurrence of the ophiuroid brittle star *Amphiura filiformis*. A transitional *N. nitidosa–A. filiformis* community was detected in the central part. Moreover, the southern part is characterised by a high abundance of *A. filiformis* and its commensal bivalve *Kurtiella bidentata*. The high number of *A. filiformis* feeding arms (up to ca. 6,800 per m^2) can largely explain the gentle change of backscatter intensity along the tracks, because sediment composition and/or seafloor structures showed no significant variability.

Introduction

Over the last 30 years the human impact on the seafloor of the North Sea has strongly increased. This includes the exploration of oil and gas fields, sand mining for construction, the installation of underwater cables and pipelines, the construction of foundations for offshore wind farms, as well as fishing by bottom trawls and dredging activities. In order to mitigate adverse effects on the seafloor, the European Union released the Marine Strategy Framework Directive (MSFD) in 2008, including 11 descriptors of "good environmental status". One of these is "seafloor integrity", defined as "a level that ensures that the structure and functions of the ecosystems are safeguarded and benthic ecosystems, in particular, are not adversely affected" (European Union 2008). The European Commission selected six indicators of seafloor integrity (cf. Rice et al. 2012), including the type, abundance, biomass and areal extent of relevant biogenic substrates. To date, regular monitoring is based largely on grab sampling, associated with time-consuming biological analyses. Another major drawback

✉ Peter Holler
peter.holler@senckenberg.de

1 Senckenberg am Meer, Department for Marine Research, Südstrand 40, 26382 Wilhelmshaven, Germany

2 Alfred Wegener Institut, Helmholtz Zentrum für Polar- und Meeresforschung, Wattenmeer Station Sylt, Hafenstrasse 43, 25992 List, Germany

3 Landesamt für Landwirtschaft, Umwelt und ländliche Räume, Hamburger Chaussee 25, 24220 Flintbek, Germany

is the point-type nature of such information, the full spatial coverage of habitats being mostly extrapolated.

Over the last decade, developments in hydroacoustic methods have enabled extensive seafloor mapping in a relatively short time period—for sidescan sonar, up to 67 km^2/day (Kenny et al. 2003). The backscatter signal reflects several abiotic properties such as surface roughness and grain size (e.g. Collins and Galloway 1998; Bornhold et al. 1999; Preston et al. 2004; Ferrini and Flood 2006; Markert et al. 2013), as well as benthic faunal elements such as mussel beds and shell debris (e.g. Quester Tangent Corporation 2003; Wienberg and Bartholomä 2005; van Overmeeren et al. 2009), coral reefs (e.g. Gleason et al. 2006; Gleason 2009), and macroalgae and seaweed (e.g. Preston 2006; Hass and Bartsch 2008; Mielck et al. 2014). In the Belgian sector of the southern North Sea, for example, Degraer et al. (2008) detected reefs of the polychaete *Lanice conchilega* by means of high-resolution sidescan sonar. This polychaete forms tubes composed of sand grains and shell fragments, which cause an increased reflectivity appearing as a patchy and grainy acoustic facies.

For the German Bight in the southern North Sea, the Marine Strategy Framework Directive-related project "WIMO" ("Scientific Monitoring Concepts for the German Bight") aims to develop new concepts for the monitoring of marine habitats (for overviews, see Winter et al. 2014; Winter et al., Introduction article for this special issue). One topic focuses on the interactions of benthic macrofauna and hydroacoustic signals from single-beam echosounders, multi-beam echosounders and sidescan sonar. Based on an older sediment distribution map of Figge (1981) and survey results from earlier projects, the present study explores this aspect in the vicinity of the island of Helgoland, representing characteristic sediment types of the German Bight. Identifying surrogate hydroacoustic signatures would facilitate meaningful spatial extrapolation of point-type biological information, thereby reducing the time and costs of seafloor sampling from aboard ship. Within this context, the aims of this study are (1) to map the distribution of surficial sediments using different hydroacoustic devices in order to find the most appropriate system for this purpose, (2) to use automatic seafloor-classification approaches for seafloor segmentation into distinct classes, (3) to provide ground-truthing for the results of the classification, and (4) to compare different sediment types and backscatter signals with the spatial distribution of macrofauna communities.

Study area

According to the sediment distribution map of Figge (1981), the seafloor in the vicinity of Helgoland is the only location in the German Bight with outcropping bedrock of Palaeozoic to Mesozoic age (Spaeth 1990), interspersed with Quaternary muddy sand to sandy mud. It is typified by the well-known benthic community dominated by the brittle star *Amphiura filiformis* (e.g. Salzwedel et al. 1985; Rachor and Nehmer 2003; Kröncke et al. 2004, 2011).

The eastern border of the study area is located about 2 km west of the island of Helgoland (Fig. 1), extending approx. 17 km in a north–south direction and approx. 6 km in a west–east direction (approx. 98 km^2). Water depth varies between 17 and 54 m (Fig. 2). The easternmost part of the study area is located within the nature preservation area "Helgoland Felssockel", where human impact is restricted to lobster-pot fishing. The study area was surveyed twice from aboard the RV *Heincke* in February and November 2014, using a RoxAnn seafloor classification system (Table 1; cf. Hass et al. 2016, this volume). A subarea in the north-eastern sector of the study area (approx. 3 km long and 2 km wide, depth range 19–35 m; Fig. 3a) was selected for more detailed surveying because it includes many different habitats, some of them difficult to evaluate with hydroacoustic gear because of steep slopes and large boulders.

Materials and methods

Acoustic data

The subarea was surveyed 11 times between 2011 and 2014 by means of seven acoustic devices from aboard the RV *Senckenberg*, RV *Heincke* and RV *Haitabu* (Table 1). Simultaneous data collection was by means of a Furuno FCV 295™ or FCV 1000™ single-beam echosounder (SBS), a Reson SeaBat 8125™ multi-beam echosounder (MBES) and a Benthos 1624™ sidescan sonar (SSS) from aboard the RV *Senckenberg*, a RoxAnn™ system from aboard the RV *Heincke*, and an Echoplus system from aboard the RV *Haitabu*.

Onboard the RV *Senckenberg*, the FCV 295 single-beam echosounder was operated with a pole-mounted Furuno 200–8B transducer. The FCV 1000 single-beam echosounder was connected to a hull-mounted Furuno 200–8B transducer with a beam angle of 7.4° at 6 dB, an emission power of 1 kW, and a pulse length of 0.5 ms. A recording depth range of 0 to 40 m (FCV 295) or 0 to 50 m (FCV 1000) was selected. Data acquisition was carried out by QTCView 5.5™ from Quester Tangent Corporation (Victoria, BC, Canada).

The 455 kHz multi-beam echosounder Reson SeaBat 8125 was also pole-mounted on the portside of the RV *Senckenberg*. The system generated 240 beams by electronic beamforming, with a beam size of 1° along track and 0.5° across track. The opening angle of 120° enables a swath coverage of up to 3.5 times the water depth. A selected line spacing of 125 m achieved full areal coverage. The data were acquired by means of QINSY

Fig. 1 Location of the study area west of Helgoland, with the subarea (*hatched box*) selected for detailed surveying
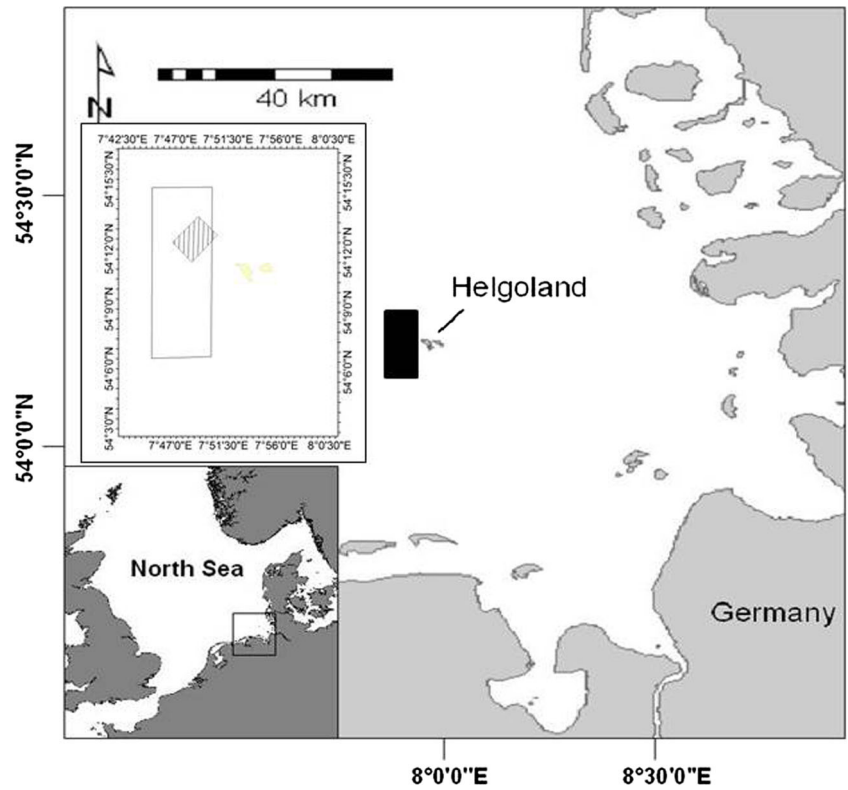
Fig. 2 Study area. *Left panel* Bathymetry (RoxAnn) and sample locations (with corresponding mean grain size). *Right panel* Interpreted and interpolated results of RoxAnn data analysis: *colour categories* see Fig. 5; *A–C* benthic communities (modified after Hass et al. 2016, this volume). *Rectangle in both panels* Subarea selected for detailed surveying
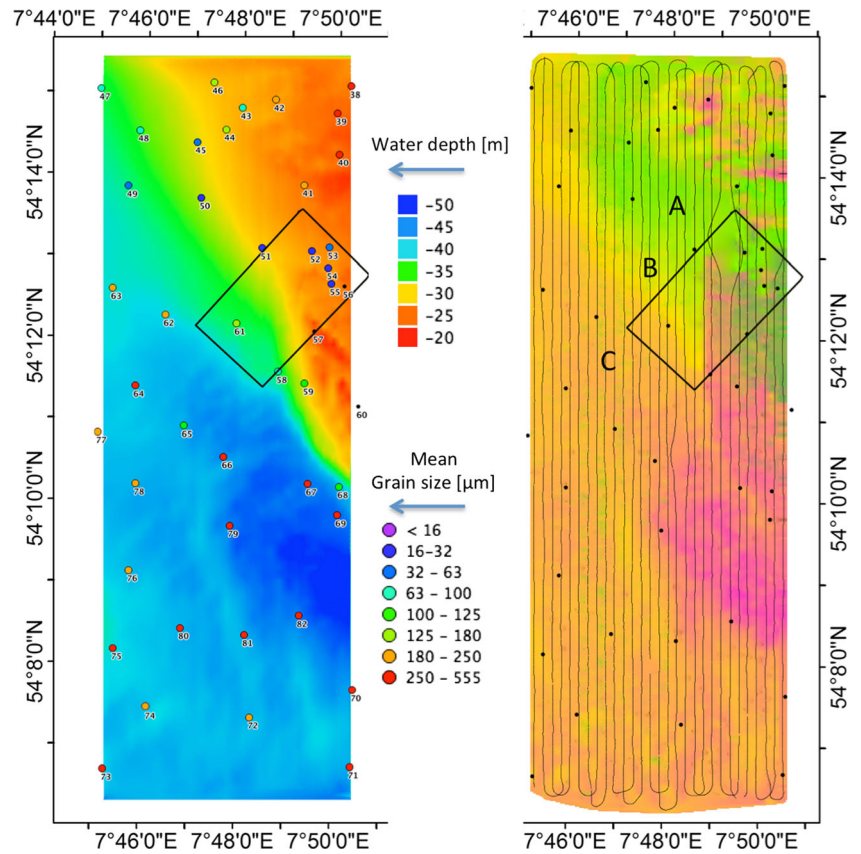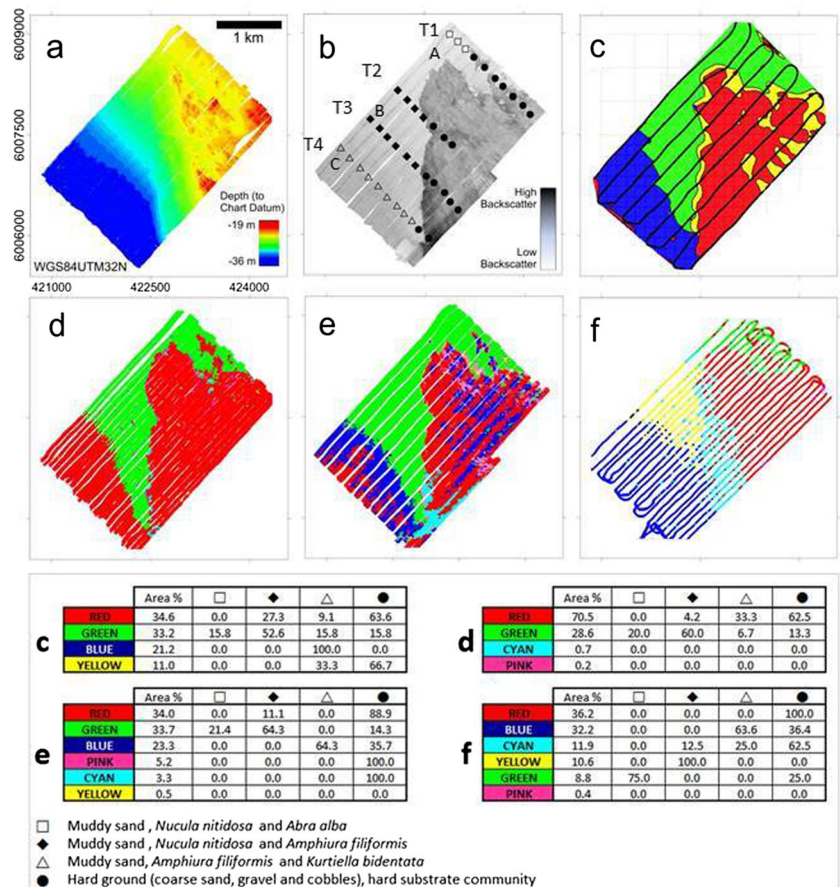
Table 1 Data acquisition between 2011 and 2014

Month/ year	Vessel	Area	Sidescan sonar	Single-beam echosounder	Multi-beam echosounder	UW-TV	Grab sampling	Macro-benthos
07/2011	RV Senckenberg	Subarea	x	x	x		x	x
08/2011	RV Haitabu	Subarea		x		x		
09/2011	RV Heincke	Subarea		x	x			
07/2012	RV Senckenberg	Subarea	x	x	x			
07/2013	RV Senckenberg	Subarea	x	x		x	x	x
10/2013	RV Heincke	Subarea		x			x	
11/2013	RV Heincke	Subarea					x	
11/2013	RV Senckenberg	Subarea			x			
02/2014	RV Heincke	Total area		x	x			
07/2014	RV Senckenberg	Subarea	x	x	x	x	x	
11/2014	RV Heincke	Total area		x	x	x	x	

version 7.1 software, the post-processing comprising a digital elevation model (DEM) with a grid size of 0.5 m. Further

interpretation is based on the ArcGIS toolbox Bottom Terrain Modeller (Wright et al. 2005). For the subarea, this entailed

Fig. 3 Subarea. Bathymetry (2012) from multi-beam echosounder (**a**) and backscatter (2011) from sidescan sonar (**b**) with positions of 2011 grab samples and macrobenthos communities. **c–f** Seafloor classification: **c** single-beam echosounder, RoxAnn GD-X (HE 364, 2011); **d** multi-beam echosounder (2012), QTC swathview; **e** sidescan sonar (2011), QTC swathview; **f** single-beam echosounder (2012), QTC 5.5/QTC Impact. *Lower panels* Corresponding areal percentages of seafloor classes and percentages of macrobenthic communities

	Area %	☐	◆	△	●
RED	34.6	0.0	27.3	9.1	63.6
GREEN	33.2	15.8	52.6	15.8	15.8
BLUE	21.2	0.0	0.0	100.0	0.0
YELLOW	11.0	0.0	0.0	33.3	66.7

(c)

	Area %	☐	◆	△	●
RED	70.5	0.0	4.2	33.3	62.5
GREEN	28.6	20.0	60.0	6.7	13.3
CYAN	0.7	0.0	0.0	0.0	0.0
PINK	0.2	0.0	0.0	0.0	0.0

(d)

	Area %	☐	◆	△	●
RED	34.0	0.0	11.1	0.0	88.9
GREEN	33.7	21.4	64.3	0.0	14.3
BLUE	23.3	0.0	0.0	64.3	35.7
PINK	5.2	0.0	0.0	0.0	100.0
CYAN	3.3	0.0	0.0	0.0	100.0
YELLOW	0.5	0.0	0.0	0.0	0.0

(e)

	Area %	☐	◆	△	●
RED	36.2	0.0	0.0	0.0	100.0
BLUE	32.2	0.0	0.0	63.6	36.4
CYAN	11.9	0.0	12.5	25.0	62.5
YELLOW	10.6	0.0	100.0	0.0	0.0
GREEN	8.8	75.0	0.0	0.0	25.0
PINK	0.4	0.0	0.0	0.0	0.0

(f)

☐ Muddy sand , *Nucula nitidosa* and *Abra alba*
◆ Muddy sand , *Nucula nitidosa* and *Amphiura filiformis*
△ Muddy sand, *Amphiura filiformis* and *Kurtiella bidentata*
● Hard ground (coarse sand, gravel and cobbles), hard substrate community

calculations of bathymetric position indexes (BPIs), bottom slopes and terrain ruggedness from the bathymetric grid (Fig. 3a).

According to Verfaillie et al. (2007), the BPI is a "measure which allows calculating where a certain location with a defined elevation is relative to the overall landscape". The BPI algorithm compares each cell elevation to the mean elevation of the surrounding cells (Verfaillie et al. 2007). It can be calculated on a broad scale (B BPI) or on a fine scale (F BPI). Negative BPI values correspond to depressions, whereas positive BPI values correspond to crests. BPIs of zero are found for constant slopes and flat areas.

The Benthos SIS 1624 sidescan sonar had a high-frequency chirp signal of 370–390 kHz and a low-frequency chirp signal of 110–130 kHz. The low-frequency beam size was 0.5° (horizontal) and 55° (vertical), whereas the high-frequency beam size was 0.5° (horizontal) and 35° (vertical). The low-frequency data were used for automatic seafloor classification. A range of 100 m (200 m swath coverage) was selected for the 2011 and 2012 surveys, and of 150 m (300 m swath) for the 2013 and 2014 surveys. Sidescan sonar data were collected along all multi-beam echosounder lines (line spacing of 125 m) at a tow speed of 5 knots and a constant tow depth of ca. 7 m below the sea surface. Tow-fish positioning was based on layback measurements. The horizontal range resolution of chirp systems is defined as (pulse length×speed of sound)/2 with pulse length=1/bandwidth. For the Benthos 1624 system (bandwidth 20 kHz, pulse length 0.00005 s) and a speed of sound of 1,500 m/s, a range resolution of 3.075 cm is calculated. The along-track resolution is defined by the vessel speed and ping rate of the sidescan sonar (BSH 2016). At a sidescan range of 100 m, 7–8 pings are emitted each second. This leads to an along-track resolution of ca. 0.35 m at a vessel speed of 5 knots (ca. 2.5 m/s). For the 150 m range setting, the maximum ping rate of five beams per second results in an along-track resolution of 0.5 m at a vessel speed of 5 knots (2.5 m/s). The backscatter data are displayed as a grey scale comprising 256 values, where 0 is assigned to black, corresponding to strong backscattering, and 255 to white, corresponding to low backscattering.

The RoxAnn (SONAVISION) system has a Furuno LS-6100 fish-finder equipped with a 200 kHz FCV 1100 transducer (beam angle: 10°) mounted on a frame in the moon pool of the RV *Heincke*. The depth range was set to 80 m. All other settings were according to the manufacturer's recommendations. A calibration cycle was run prior to the measurements. The data were recorded using the RoxAnn acquisition software RoxMap 32 (SONAVISION, Aberdeen, UK) at a line spacing of 220 m.

The EchoPlus system is permanently installed onboard the RV *Haitabu*, connected to a Fahrentholz Lithugraph XL echosounder. The working frequencies were 30 and 200 kHz. The data were recorded using JEDI software that is customer programmed for the Landesamt für Landwirtschaft, Umwelt und ländliche Räume, Flintbek, Germany. In contrast to the other single-beam echosounder classification systems (RoxAnn and QTC5.5), the classification of EchoPlus data was in the supervised mode with a line spacing of 250 m.

In order to compare the results of seafloor classification systems quantitatively, two approaches are commonly used. As outlined in Schimel et al. (2010a, b), the conventional approach is to produce a case study map for each classification, followed by estimates and comparison of their accuracy based on ground-truthing data (see, for example, Brown et al. 2005; Lucieer 2008; Brown and Collier 2008). The other approach is a comparison of one map with another without referring to ground-truthing data. This approach is very valuable for the determination of similarities between the different classifications, but no information regarding map accuracy is gained. This kind of comparison of similarities is normally calculated using error matrices (Schimel et al. 2010a, b).

The present ground-truthing datasets are based on sidescan sonar data from the subarea (ca. 6 km^2), and the classification patterns for the different methods look very similar (cf. above). Therefore, similarity was not calculated by means of error matrices but rather by the Bray-Curtis similarity index of degree of areal coverage (Fig. 3c–f) using the PAST software package (Hammer et al. 2001). The software computes a number of similarities between all pairs of rows entered. The results are given as a symmetric similarity matrix.

Grab sampling

In 2011 surface samples were collected from aboard the RV *Senckenberg* by means of a 0.1 m^2 Van Veen grab at 39 sites along four transects in the subarea selected for more detailed exploration. At each site, three replicates were taken for macrofauna and sedimentological analyses (Fig. 3b). Transect locations were chosen using a preliminary sidescan sonar mosaic in order to make sure that all different backscatter areas were sampled.

The 2013 survey concentrated on sampling sites characterised by fine-grained sediments (e.g. muddy sand), with an additional transect at the southern border of the subarea. Here, three additional samples were retrieved from aboard the RV *Heincke* (11/2013) using a spade-box corer (50×50×60 cm) at sites where high abundances of *A. filiformis* were determined in 2011.

During the 2014 survey of the RV *Senckenberg*, 40 grab samples for sedimentological analyses were retrieved by a Shipek grab. During the 2014 survey with the RV *Heincke*, samples from 44 sites were taken from the total study area using a HELCOM 0.1 m^2 Van Veen grab. Of these, 41

samples were retained for sediment analyses, three locations being characterised by stones.

Macrofauna and sediments

At all locations where samples for macrofauna analyses and sedimentological analyses were retrieved, three grabs were taken at each location. Two of the grabs were used for macrofauna analyses and one grab for sedimentological analyses. The average distance between replicates is estimated to range between 15 and 30 m (Capperucci and Bartholomä 2012).

For sediment analyses, a macroscopic description and photographic documentation of the sediment surface were conducted for each grab. Then, subsamples of surface sediments were taken for grain-size analyses. The upper 2 cm was chosen because this depth interval is close to the penetration of the high-frequency acoustic signal into sandy sediments (Huff 2008; 1.5 cm for 500 kHz). In the laboratory, the samples were desalted in semi-permeable hoses over 24 h. Each desalted sample was washed through a 0.063 mm mesh screen to separate the mud fraction (<0.063 mm). The coarse fraction was then dried and dry-sieved through a 2 mm mesh. Shell debris and gravel were weighed in order to determine the gravel content (>2 mm) as well as the content of shell debris >2 mm. The coarse fraction (>2 mm) was not further analysed. The sand size fraction (0.063 to 2 mm) was weighed, treated with hydrochloric acid, and weighed again to determine the content of sand-sized shell debris. For the total amount of shell debris of the samples (see ESM Table 1, parts a and b, in the electronic supplementary material available online for this article), the shell debris of the gravel size fraction and the sand size fraction were summed up. The sand fraction was split into 1/4 Φ units ($\Phi = -\log2$ diameter of particle in mm) from −1 to 4 Φ, using calculations from settling velocities measured by a MacroGranometer™ settling tube (Flemming and Thum 1978; Tucker 1988). The mud fraction was analysed using a Micromeritics SediGraph III 5120™ (Stein 1985).

Samples HE416-38 to 82 were photographed and macroscopically analysed. At every sampling location the underwater video set was deployed to produce high-definition videos of the seafloor at the sampling location. In the laboratory the samples were treated with acetic acid to remove carbonates and with hydrogen peroxide to remove organic compounds. After the chemical treatment the fraction >2,000 μm was separated and the fraction <2,000 μm was measured in 100 size fractions using the CILAS particle sizer. Then the data were processed and re-sampled in 10th phi steps.

For macrofauna analyses, each 0.1 m^2 Van Veen grab was sieved onboard ship at 1 mm mesh size and the retained material was fixed with 4% buffered formalin. Samples of coarse-grained sediments were decanted 10 times while sieving. In the laboratory, organisms were stained with Rose Bengal and identified to species level.

Data analyses

RoxAnn- and EchoPlus-based seafloor classification

The RoxAnn and EchoPlus theory of operation is to release an initial sound pulse and to take the energy received in the electronically gated last third of the first echo return (E1) as a measure of seafloor roughness. The rougher the seafloor, the more energy is received back and the longer becomes the tail of the echo. All of the energy received with the second echo return (E2, after reflection at the sea surface and again at the seafloor) is a measure of seafloor hardness. The amount of reflection is controlled by the difference in acoustic impedance between seawater and the seafloor (Chivers et al. 1990; Schlagintweit 1993; Dean et al. 2013). Adverse effects due to changing water depth, such as variations in the backscatter amplitude and the tail length of the return signals, are electronically compensated by a pulse-integration constant. This constant adjusts the total integral value of the E1 and E2 gate areas. RoxAnn uses TVG (time-varied gain) to compensate for spreading loss with increasing water depth (Chandu, SonaVision, pers. comm., 2014).

The E values are given in DC voltage, and measurements were taken every second. Each data line includes the geographic position, date and time, water depth, as well as E1 and E2 values. Whenever either one of the variables did not record or showed implausible data (outliers), the whole data line was removed from the dataset during data processing.

The resulting data were colour coded using 10,000 RGB bins in the E1/E2 space. Each colour band (R, G and B) was then separately interpolated using the "natural neighbour" method. After interpolation, the three colour bands were recombined, resulting in an RGB triplet for every data point on the interpolated grid. Since the colour values depend on the two variables E1 and E2, the legend for the map is also two-dimensional. All data processing and graphics were produced using self-programmed MATLAB-based scripts and Quantum GIS 2.4.0-Chugiak. The JEDI software serving to record the Echoplus E1 and E2 data also allows a supervised classification, based on ground-truthing data entered into the system. However, in the context of this study, only the raw E1 and E2 data were used.

QTC-based acoustic seafloor classification

Based on promising findings of previous work in the southern North Sea (Wienberg and Bartholomä 2005; Bartholomä 2006; Bartholomä et al. 2011), Quester Tangent™ software was used for the acoustic seafloor classification. Full wave forms of single-beam echosounder data were collected and analysed with QTC 5.5™/QTC Impact™. Sidescan sonar and multi-beam echosounder backscatter data were classified using QTC Swathview, with processing steps including data

cleaning, and compensation for depth, range and insonification angles. After compensation, the time-series data from the single-beam echosounder were aligned by their bottom picks and summed in stacks of five. The analyses of the echo shape using QTC proprietary algorithms generated 166 so-called full feature vectors (FFVs). With sidescan sonar and multi-beam echosounder images, borders of rectangular patches were distributed over the unmasked regions of backscatter images. In order to shorten the processing time of the backscatter data, a reduced number of only 29 FFVs were extracted, comprising basic features (1–4), grey level co-occurrence matrix (GLCM) data (5–20), circular Fourier transformation data (21–28) and fractal dimension data (29): *1–4* mean, standard deviation, skewness, kurtosis; *5–8* GLCM correlation; *9–12* GLCM contrast; *13–16* GLCM entropy; *17–20* GLCM homogeneity; *21–28* circular Fourier transform; *29* fractal dimension (QTC, pers. comm.).

Further processing of the amplitude data for single-beam echosounder records as well as for image data for sidescan sonar and multi-beam echosounder data was exactly the same for all systems. For all hydroacoustic datasets, PCA (principal component analysis) was used to reduce the FFVs (166 FFVs for single-beam data, 29 FFVs for multi-beam and sidescan sonar data) to three components, i.e. Q1, Q2 and Q3. These were plotted in three-dimensional space (Q space) and used for clustering (Preston et al. 2004).

Segmentation was done in the three-dimensional space of the Q values. Starting with all records in the same class, a variant of the k-means clustering method separated them into clusters, i.e. acoustic classes. The result of the k-means clustering is presented graphically as score against number of classes. The score is a statistical measure of cluster size and tightness (Quester Tangent Corporation 2011). The statistically optimal number of classes is characterised by the minimum score. Each record, originating from a stack of single-beam echoes or from the amplitudes in a rectangle, was assigned to the closest class centre in the Q space in a process that was iterative and stable. According to QTC, each cluster represents an acoustically distinct area. The QTC seafloor classes files were gridded (nearest neighbour method) using a grid size of 1 m in QTC Clams™ software. This software also allows a categorical interpolation to extend point and line coverage to full coverage. The full coverage data was saved in the Geotif format for further analyses.

The final Geotif file was imported into a geographic information system (ArcGIS 10.3™) to generate maps of acoustic classes. In this GIS environment, the macrofauna clusters and sediment data were combined with the acoustic map for validation of the acoustic classes.

Macrofauna

The software PRIMER v6 (Plymouth Marine Laboratory; Clarke and Gorley 2006) was used for statistical analyses of macrobenthos data. Diversity was analysed according to Shannon and Weaver (1949) and the Pielou (1969) evenness index. For multivariate analyses, the data were fourth root transformed and the Bray-Curtis similarity coefficient (Bray and Curtis 1957) was calculated. Cluster analyses were performed to detect similarities between communities. Significant differences between communities were evaluated by means of the ANOSIM randomisation test (Clarke and Green 1988). SIMPER was used to detect the characteristic species per community (Clarke and Warwick 2001).

Results

Acoustic backscattering

In the subarea, the sidescan sonar backscatter mosaic of 2011 (Fig. 3b) shows two main zones of different seafloor backscatter. A zone of generally higher backscatter (darker grey tones) extends from the north-eastern boundary of the subarea and generally dominates the eastern sector, with grey values varying between ca. 47 and 200 (average of 160). The northern, north-western and southern sectors display lower backscattering intensity with grey values of ca. 170–240 (mostly 200–210). Within the zone of weaker backscatter, a slight increase in grey tones is visible from the northeast to the southwest (Fig. 3b). The grey values decrease from ca. 230 near the north-eastern boundary (A in Fig. 3b) to ca. 210 in the centre (B in Fig. 3b) and 170–180 near the south-western boundary (C in Fig. 3b) of the subarea (Table 2). Although the absolute grey values for the years 2012 and 2014 are slightly different because of different environmental settings such as wave height and wave direction, the general increase of backscatter strength from the northeast to the southwest is confirmed for both surveys of 2012 and 2014 (Table 2).

Table 2 Grey values (0=black, 255=white) for sidescan sonar mosaics from 2011 to 2014 in the subarea
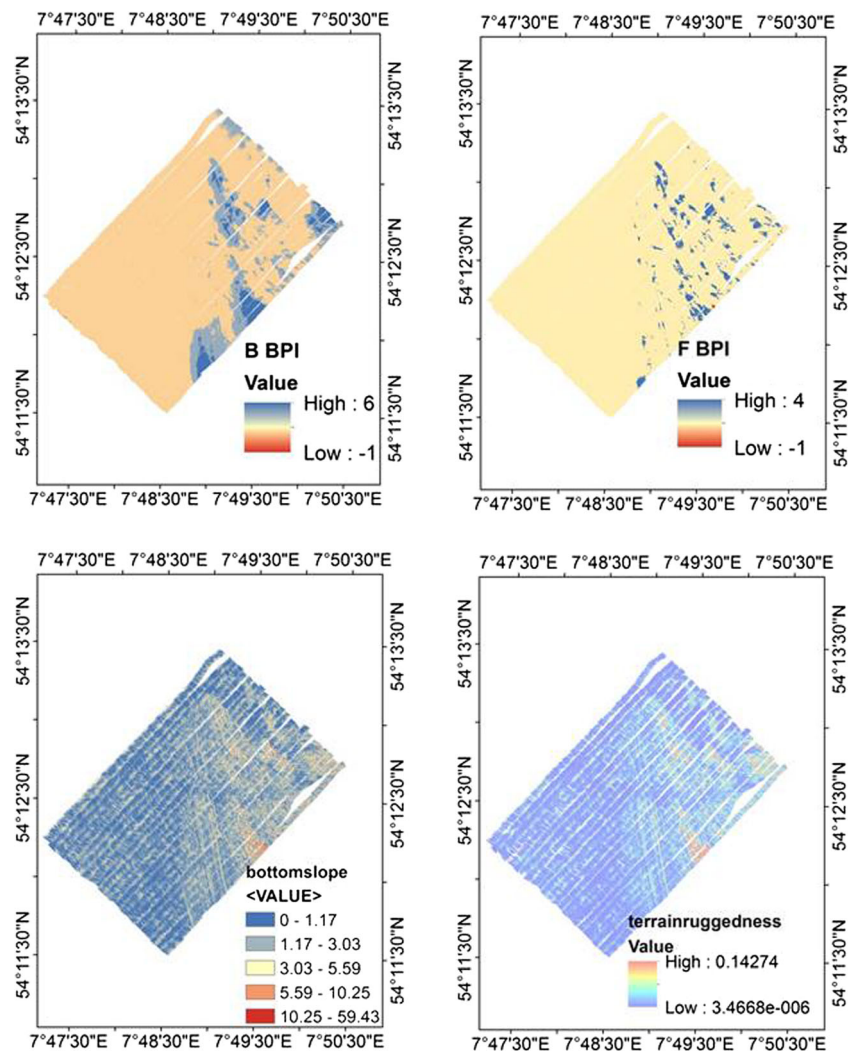
	A	B	C
2011	230	210	170
2012	210	200	170
2013	235	225	200
2014	250	248	168

Derivates from bathymetry

In the subarea, the broad-scale BPI values (Fig. 4, upper left) vary between −1 and 6. However, the strongest variation of BPIs is found in the north-eastern sector with a stronger back-scattering of sidescan sonar data (Fig. 3b). This sector is also characterised by stronger variations in bathymetry (Fig. 3a). The remaining sectors show a BPI of zero, indicating a flat seafloor or a constant slope. The fine-scale BPI values (Fig. 4, upper right) show variations between −1 and 4, with most values being zero. Again, the strongest variations are visible in the north-eastern sector of the subarea.

The bottom slopes (Fig. 4, lower left) vary between 0° and 59°. Again, the higher values are restricted to the northeast of the subarea, whereas gentler slopes (0–1.1°) were recorded in the remaining sectors. The calculated terrain ruggedness (Fig. 4, lower right) mirrors the results of the other bathymetry derivates (BPI, bottom slopes), with higher values in the north-eastern sector of the subarea and lower values in the remaining sectors.
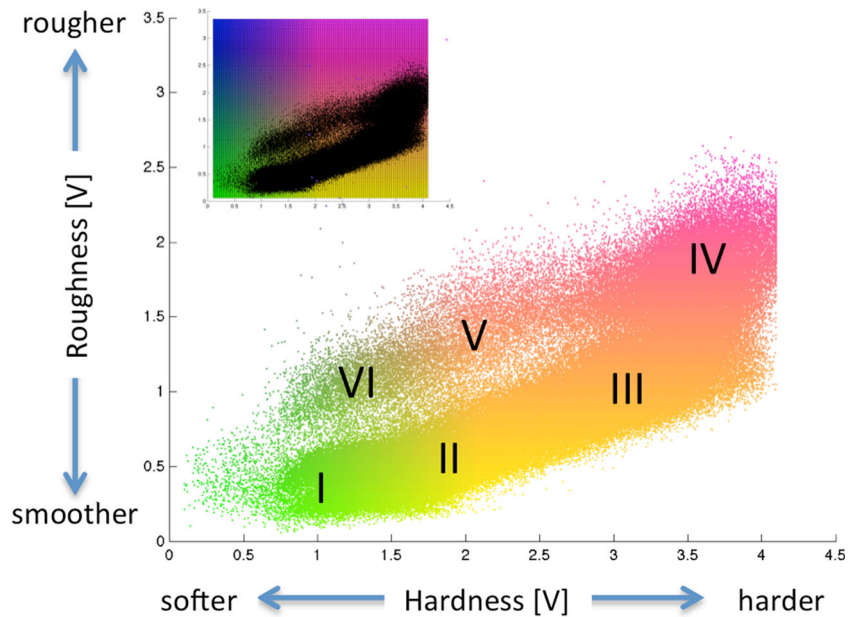
Acoustic seafloor classification

QTC Swathview™ sidescan sonar

In the subarea, segmentation of the acoustic backscatter data from sidescan sonar by QTC Swathview™ resulted in six seafloor classes (Fig. 3e). The areal distribution of seafloor class green (coverage: 33.7% of the seafloor) coincides with the areas of light grey tones on the sidescan sonar mosaic (Fig. 3b). Therefore, this class is related to low backscatter values (grey tones: 210–250) of the sidescan sonar signal. Seafloor class red (coverage: 34% of the seafloor, Fig. 3e) correlates well with high backscatter values (grey tones: 168–200) of the sidescan sonar data in the central and south-eastern sectors of the subarea, but occurs also in the southern and south-western sectors where low backscatter values are visible on the sidescan sonar mosaic (Fig. 3b).

In the central and south-eastern sectors of the subarea, sea-floor class blue (coverage: 23.3% of the seafloor) is visible near the nadir of the sidescan sonar data (Fig. 3b). This

Fig. 4 Subarea. Broad-scale bathymetric position index (BPI, *upper left*), fine-scale BPI (*upper right*), bottom slope (*lower left*) and terrain ruggedness (*lower right*)

Fig. 5 Study area. RoxAnn box of roughness (E1) vs. hardness (E2). *I–V* Classes mentioned in the text. *Inset* E1 vs. E2 plotted as black dots superimposed on the chosen colour scheme (modified after Hass et al. 2016, this volume)

suggests either that class blue is a classification artefact, due to the generally stronger backscatter signal close to the nadir, or that variations in seafloor cover (e.g. different types/amounts of epifauna) may have generated this class. However, in the southern and south-western sectors, the blue class (Fig. 3e) correlates well with a slight increase in backscattering intensity seen in the sidescan sonar mosaics (Fig. 3b). Seafloor class cyan (coverage: 3.3% of the seafloor) is predominantly visible in the south-eastern sector with high backscatter values. The remaining two classes yellow (coverage: 0.5% of the seafloor) and pink (coverage: 5.2% of the seafloor) occur in small patches mostly in and around the areas of high backscatter in the sidescan sonar signal (Fig. 3b).

QTC Swathview™ multi-beam echosounder

In the subarea, backscatter data of the multi-beam echosounder were segmented into four acoustic seafloor classes using the QTC Swathview™ software. Most of the subarea is characterised by only two classes (Fig. 3d): red and green. Class green covers 28.6% of the seafloor, coinciding with areas of low backscatter values in the sidescan sonar mosaic (Fig. 3b). Seafloor class red covers 70.5% of the seafloor, coinciding with areas of strong seafloor backscattering in the central and south-eastern sectors of the subarea but also in the southern and south-western sectors where a gentle increase in backscatter values is visible. The seafloor class cyan (coverage: 0.7% of the seafloor) is constrained within the area of high backscatter values, whereas the remaining class pink (coverage: 0.2%) is disseminated over the whole subarea and might be due to classification of noise.

RoxAnn

The E1/E2 data from the RoxAnn system were processed by means of two classification approaches. In the subarea, fuzzy seafloor classification (Fig. 3c) reveals four classes. Class red covers 34.6% of the seafloor and coincides with the area of strong backscattering in the sidescan sonar data (Fig. 3b). Class green (coverage 33.2%) corresponds to the area of weak backscattering, whereas class blue (coverage 21.2%) is associated with slightly increased backscattering in the south-western sector of the subarea (Fig. 3c). Class yellow covers 11.0% of the subarea, and mainly co-occurs with strong backscatter in the central sector (Fig. 3b, c).

For the second approach of processing (RoxProgs), the RoxAnn data are displayed in the E1/E2 space ("RoxAnn box") in Fig. 5 for the whole study area. Six acoustic classes can be distinguished. Since there are usually no sharp borders in nature, class borders were inserted neither in the RoxAnn box (Fig. 5) nor in the map (Fig. 2). If sharp borders occur, then they are clearly visible in both figures. Class I occurs exclusively above 30 m water depth. According to the RoxAnn box, the green colours suggest the softest and smoothest values of the entire dataset. Class I is largely congruent with QTC class green (single-beam echosounder as well as multi-beam and sidescan sonar) and with the areas of weakest backscatter of the sidescan sonar in the north-eastern part of the subarea. Class I demarcates a large curved sector in the upper northern part of the study area (Fig. 2).

Class II (yellow) suggests a slightly harder and rougher seafloor. It is congruent with QTC class yellow but extends further into the southern part of QTC class cyan. Class III (orange) largely resembles QTC class blue; however, parts

of the subarea in the south and southeast covered by QTC class blue belong more to RoxAnn class II (i.e. revealing lower roughness and hardness values than class III). Class III demarcates large sectors in the southern and western parts of the study area (Fig. 2), associated with slightly increased backscatter in the sidescan sonar records. Class IV has hardness values similar to class III but associated with clearly higher roughness values. Class IV shows reddish colours and is congruent with QTC class cyan. It covers a large part of the eastern sector of the study area. Classes V and VI are congruent with QTC class red. They encompass the hardness values of classes I, II and partly III. However, the roughness values are significantly higher and classes V and VI are clearly separated from classes I to III. They cover a distinct sector in the central eastern part of the study area.

QTC View 5.5™/QTC Impact™ single-beam echosounder

In the subarea, the single-beam echosounder data can be subdivided into six statistically significant different acoustic seafloor classes (Fig. 3f). The sector characterised by low backscatter values of the sidescan sonar mosaic is covered by seafloor classes green (coverage: 8.8% of the seafloor) and yellow (coverage: 10.8%). Seafloor classes red (coverage: 36.2%) and cyan (coverage: 11.9%) are predominantly restricted to the central and south-eastern sectors of the subarea where high backscatter values are visible on the sidescan sonar mosaic (Fig. 3b). The southern and south-western sectors, where the sidescan sonar mosaic shows slightly increased backscatter values, have seafloor class blue (coverage: 32.2%). Seafloor class pink covers only 0.4% of the seafloor and is mainly situated within seafloor class red in the central part of the subarea (Fig. 3f).

Sediments

In the subarea, the locations of sediment samples in 2011 were determined on the sidescan sonar backscatter mosaic in order to ensure full coverage of backscatter signatures (Fig. 3b). In assessing the whole study area, sample locations of survey HE416 in 2014 were chosen on the basis of RoxAnn measurements (Fig. 2).

According to the classification of Folk (1954), the seafloor samples range from gravel to sandy mud (ESM Table 1 in electronic supplementary material). In the subarea, most samples are classified as muddy sand (26 of 38 samples). For the whole study area, five samples are classified as gravel (samples 09, 45, 71, 72, 73), three as sandy mud (samples 10, 69, 70), two as muddy gravel (samples 46 and 47), one as gravelly muddy sand (sample 08) and one as muddy sandy gravel (sample 95). Grab samples characterised by high amounts of gravel contained not only granules (diameter 2–4 mm) but also pebbles (4–64 mm) and cobbles (64–256 mm; cf.

Wentworth scale; Wentworth 1922; Krumbein and Aberdeen 1937).

Coarser-grained sediments were retrieved from the central and south-eastern sectors of the subarea, and finer-grained sediments from the northern, southern and south-western sectors (Fig. 3b). In the latter, there are only small variations in grain size distributions from the northeast to the southwest (Fig. 6). Using the Folk (1954) classification, all samples (2011_02, 2011_42, 2011_64, 2011_86) are muddy sand. However, using the phi mean of the sand size fraction of these samples (Fig. 6) and the Wentworth (1922) scale, sample 2011_86 (phi mean 2.601) can be classified as muddy fine sand. According to this classification, the remaining samples are muddy very fine sand (phi mean 3.463–3.491). Samples from almost the same locations in the 2013 survey (from northeast to southwest: 2013_20, 2013_17, 2013_14, 2013_02) yielded the same results. The southernmost sample (2013_02) is classified as muddy fine sand, whereas the remaining samples are muddy very fine sand (Fig. 7).

Regarding the whole study area, there are similar spatial distribution patterns of hardness- and roughness-based classification (ESM Table 1, part c, in electronic supplementary material; Fig. 2). However, this dataset also highlights the patchy character of the area. The sediment becomes generally slightly coarser from north to south. The elevation highs in the NE of the study area reveal pebbles and boulders that inhibited the use of a grab sampler (HE416_56, 57, 60), as well as medium sands (HE416_38–40) and muddy sediments (HE416_47–55). The deeper southern third of the study area is characterised by sandy sediments throughout.

Macrofauna

In the samples from 39 stations taken in 2011 in the subarea, 189 macrofauna taxa were identified, comprising mostly molluscs (49%) followed by annelids (23.7%), echinoderms (18.6%) and crustaceans (7%). The four transects T1 to T4 (Fig. 3b) show a variation of the main macrofauna groups. The abundance of molluscs decreases from T1 to T4, whereas that of echinoderms increases (Fig. 8). Despite the high sedimentary diversity, the cluster analyses provided only four significantly different macrofauna communities (Fig. 9) based on the ANOSIM test (global R value of 0.92, significance level of 0.1%).

The three stations of community A (1–3) are in the northern part of the subarea (Fig. 3b). According to the cluster analyses, this is a *Nucula nitidosa–Abra alba* community associated with polychaetes such as *Lagis koreni* and *Scalimbregma inflatum*. This community has a mean taxa number of 40/0.1 m^2, a mean Shannon index of 2.18, a high mean evenness (0.59), and the highest mean abundance (11,627 ind./m^2). Community A is associated with the acoustic class green (sidescan sonar, multi-beam echosounder, single-beam
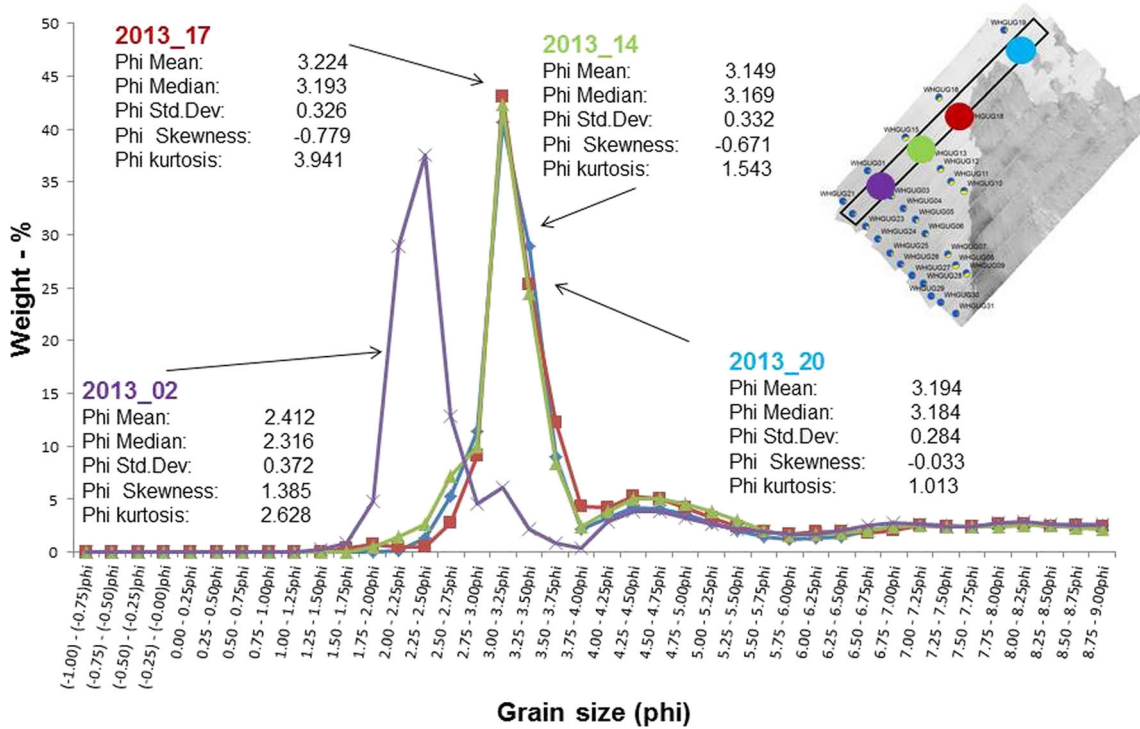
Fig. 6 Subarea. Grain size distributions along the transect of 2013 from the northwest (sample 2013_20) to the southwest (sample 2013_02)

echosounder QTC) or class I (single-beam echosounder RoxAnn; Fig. 3c–f, ESM Table 2 in the electronic supplementary material).

Stations belonging to community B are in the centre of the subarea (Fig. 3b), earmarked by muddy sand to sandy mud. Dominant species are *N. nitidosa*, *A. filiformis* and *Hyala*
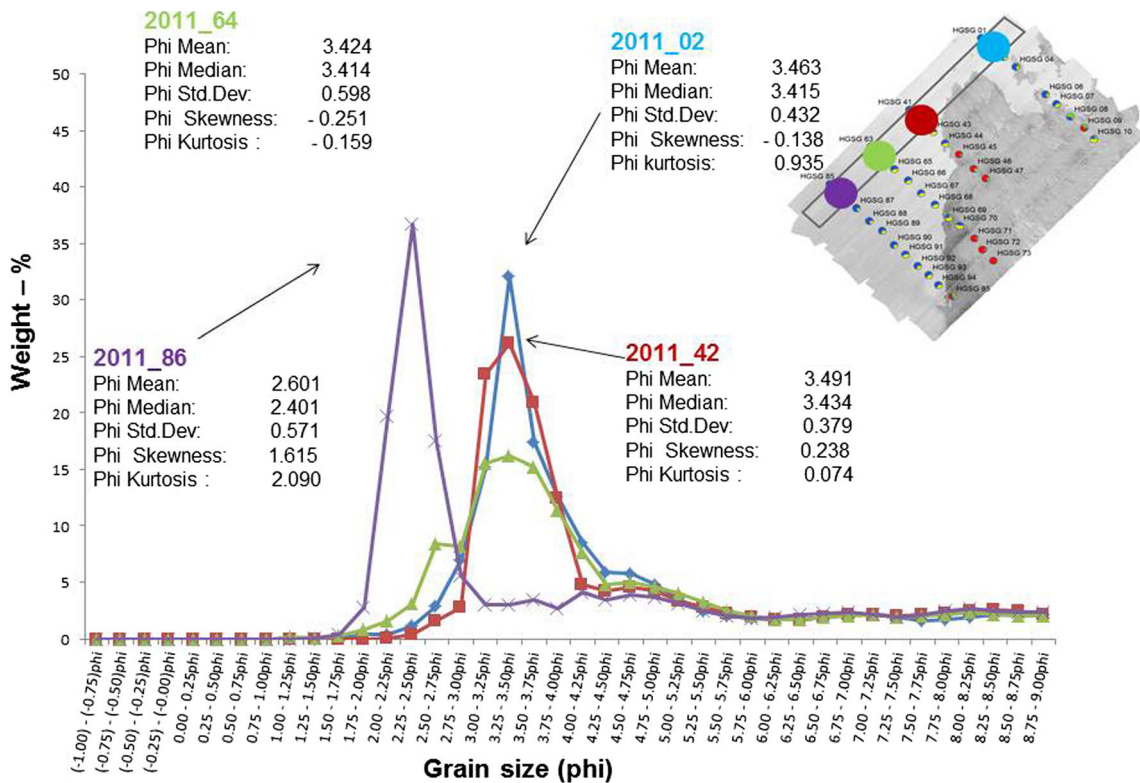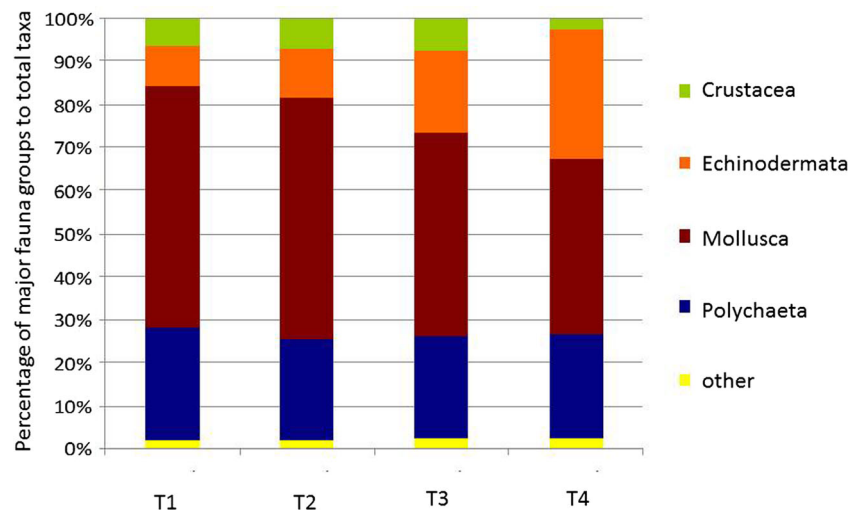

Fig. 7 Subarea. Grain size distributions along the transect of 2011 from the northwest (sample 2011_02) to the southwest (sample 2011_86)

Fig. 8 Subarea. Percentage of major fauna groups to total taxa along transects T1 to T4 (for locations of T1–T4, see Fig. 3b)

vitrea. This community comprises species of both communities A and C, although in lower abundances—mean abundance of 5,160 ind./m², mean taxa number of 37/0.1 m², and highest mean Shannon index (2.48) and evenness (0.69; Fig. 3c–f, ESM Table 2 in electronic supplementary material). Community B is associated with the acoustic class green (QTC sidescan sonar, QTC multi-beam echosounder), the class yellow (QTC single-beam) and the RoxAnn class I.
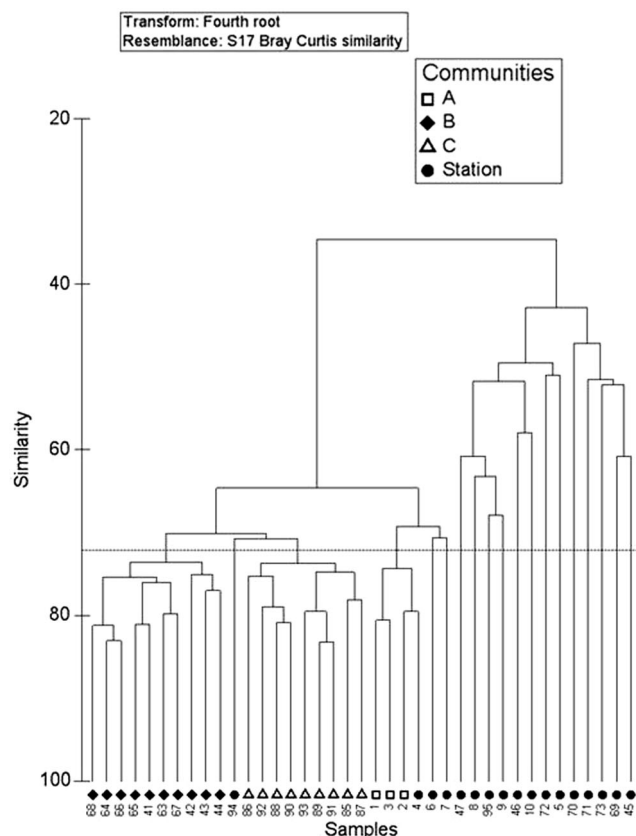
Community C is an *A. filiformis–Kurtiella bidentata* community dominated by the brittle star (1,711/m²) and commensal bivalve species. The highest mean taxa number of 42/0.1 m², mean abundance (5,702/m²), Shannon index (2.41) and evenness (0.64) were found. This community is associated with the acoustic class blue (QTC sidescan sonar), red (QTC multi-beam echosounder), QTC single-beam class blue and RoxAnn class III (Fig. 3c–f, ESM Table 2 in electronic supplementary material).

The fourth community included stations from an area of higher backscattering caused by coarser sediments with boulders and pebbles (Fig. 3b). There, a quantitative sampling with the Van Veen grab was impossible. Qualitative samples revealed typical hard-substrate organisms such as the polychaetes *Pomatoceros triqueter* and *Sabellaria spinulosa* (Hartmann-Schröder 1996), a high abundance of anthozoans, but also soft-bottom species such as *Lagis koreni*, *Gattyana cirrhosa* and *Protodorvillea kefersteini*. A similar community was found by Kühne and Rachor (1996) at the "Steingrund" near Helgoland.

To confirm the results of 2011, the *A. filiformis* data of the 2013 samples were analysed. Again, high abundances of *A. filiformis* were detected in the southern part of the subarea (see ESM Table 3 in the online electronic supplementary material).

Brittle star abundance vs. side-scan sonar grey values

An increase in the abundance of the brittle star *A. filiformis* was found from the northern to southern parts of the subarea (Fig. 8). The highest abundances were determined at stations with a water depth of about 30 m. In Fig. 10 (cf. ESM Table 3 in electronic supplementary material), the abundance of *A. filiformis* is plotted against grey values (0=black, 255=white) from the 2011 sidescan sonar mosaic (Fig. 3b).

Fig. 9 Subarea. Hierarchical clustering of macrofauna samples
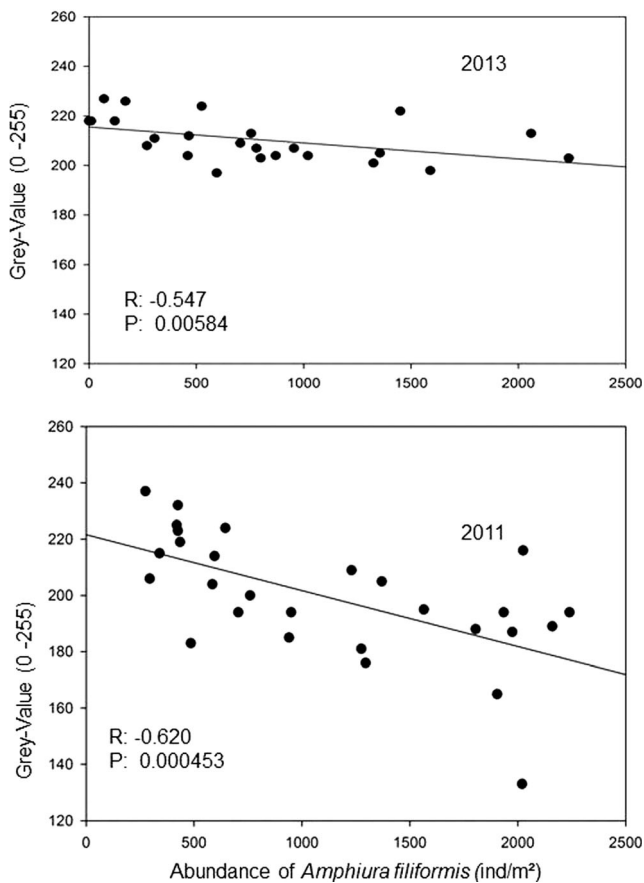
Fig. 10 Subarea. Correlations (Spearman rank order) between grey values (0=black, 255=white) from sidescan sonar mosaic and total abundance of the brittle star *A. filiformis* in 2013 (*upper panel*) and 2011 (*lower panel*)

Table 3 Similarity index of seafloor classifications based on Bray-Curtis

	RoxAnn	Multi-beam	SSS	QTC
RoxAnn	1.00	0.63	0.89	0.75
Multi-beam	0.63	1.00	0.64	0.46
SSS	0.89	0.64	1.00	0.70
QTC	0.75	0.46	0.70	1.00

The Spearman rank order (Spearman 1904) shows a negative correlation between grey scale values and abundance of brittle stars. The variation increases from 2011 to 2013 (Fig. 10).

The 2013 samples again show similar high abundances of *A. filiformis* in the southern part of the subarea (ESM Table 3 in electronic supplementary material). The correlation between grey values and the abundance of the brittle star using the Spearman rank order reveals a correlation coefficient of −0.547 and P value of 0.00584. This confirms the results for the 2011 correlation. In contrast, the sample transect added near the southern border of the subarea in 2013 (samples WHGUG21–WHGUG31) shows average mean abundances of *A. filiformis* (ESM Table 3 in electronic supplementary material).

Discussion

Acoustic seafloor classification comparison

The physical configuration of swath-based and vertical down-looking single-beam echosounders implies different types of

return signals. Therefore, the classification of swath systems is based on statistical segmentation of images, whereas the classification of single-beam echosounder data is based on the statistical analysis of the wave shape (QTC 5.5) and multiple-echo envelope analysis (RoxAnn). For all systems, a very similar classification pattern was generated (Fig. 3c–f, Table 3). The seafloor classifications obtained by the RoxAnn system and from the sidescan sonar data (QTC Swathview) show the highest similarity of 0.89, whereas there is a similarity of 0.63 for the RoxAnn and multi-beam echosounder data (QTC Swathview). The similarity between the single-beam echosounder classifications from RoxAnn and QTC 5.5 is 0.75.

The minimum similarity value was computed for the classifications of the multi-beam echosounder (QTC Swathview) and the QTC 5.5 single-beam data (0.46). The remaining similarities vary between 0.70 (QTC 5.5 and sidescan sonar) and 0.64 (sidescan sonar and multi-beam echosounder).

Generally lower similarities between classifications from single-beam echosounder data and swath systems have been noted earlier (Anderson et al. 2008; Schimel et al. 2010a, b; Bartholomä et al. 2011). Schimel et al. (2010b) pointed out that this can be at least partly explained by the differences of grazing angles between the systems. Single-beam echosounders operate at very high grazing angles only (85–90°), whereas sidescan sonar systems have low to medium grazing angles (1–45°) and most multi-beam echosounders operate from low to very high grazing angles (25–90°; Schimel et al. 2010b). Indeed, Lurton (2002) showed that the effects of surface roughness and volume backscattering vary strongly with grazing angle.

The generally lower similarity between the multi-beam echosounder classification and the classification from RoxAnn, QTC 5.5 and sidescan sonar was not expected. Preston et al. (2003), Bartholomä et al. (2011), Micallef et al. (2012), Markert et al. (2013) and Lurton and Lamarche (2015) showed that classifications obtained from multi-beam echosounder data are of superior quality. This is, among others, due to the fact that for every single beam of the multi-beam system, data on backscatter, depth and grazing angle are available for further processing (e.g. compensation). Classifications from multi-beam echosounders and sidescan

sonar systems are normally very similar because they both are based on the backscatter image (Schimel et al. 2010a).

The low similarity between the multi-beam classification (Fig. 3d) and all other classifications (Fig. 3c, e, f) is mainly caused by the areal coverage of classes green (28.6%, Fig. 3d) and red (70.5%, Fig. 3d). At the moment, it is not clear why the multi-beam echosounder classification is so different from the other classifications. The surveys were carried out in summer (July) 2011–2014, a season commonly earmarked by increased suspended particulate matter. Whether this partly impeded the acoustic energy of the high-frequency multi-beam echosounder (455 kHz) from reaching the seafloor is an aspect requiring further research. Mazel (1985) noted that suspended sediment scatters the signal on its way to the seafloor.

Influence of macrobenthos

All classification systems showed differences in acoustic results between the southern and northern parts of the subarea chosen for more detailed surveying (Fig. 3), reflected also by the occurrence of community C (ESM Table 2 in electronic supplementary material). This can be explained neither by changes in sediment composition (e.g. Riegl et al. 2007; Freitas et al. 2011) nor by variations in bathymetry.

Both single-beam systems clearly reveal changing seafloor properties between the areas inhabited by communities B and C (Figs. 2 and 3c, f). Slight differences between the results of the two systems might be due to different years and different months (seasons) in which the measurements were carried out. RoxAnn data suggest that community C also dominates large parts of the total study area (Fig. 2, orange colours). Evidently, changes in backscatter signal strength can be explained by changes in seabed roughness induced by varying abundance of the ophiuroid A. filiformis in the southern part of the study area at about 30 m depth.

The brittle star is the dominant species of soft sediments in the North Sea—e.g. the Oyster Ground (Cadée 1984; Kröncke et al. 2004, 2011) and the German Bight (Salzwedel et al. 1985; Kröncke et al. 2004, 2011). Associated species of A. filiformis communities were Harpinia antennaria and the bivalves K. bidentata and Corbula gibba (e.g. Rachor and Nehmer 2003; Reiss et al. 2006). A. filiformis is found at depths of 5 m to more than 200 m (e.g. Buchanan 1964; Künitzer 1989; Künitzer et al. 1992; Sköld et al. 1994; Rosenberg et al. 1997; Josefson 1998; Southward and Campbell 2006).

The size of the disk of A. filiformis can reach a diameter of 10 mm, and the slender, flexible arms a length of up to 100 mm. The specimens (disks) have been found buried at sediment depths of 3–8 cm (e.g. Rosenberg et al. 1997, 4 cm depth; Josefson 1998, 3–6 cm depth), depending on the age and therefore on the size of the disk and the arm length of the specimen. The three box cores taken by the RV Heincke in November 2013 from the area with high abundances of A. filiformis showed a burial depth of 5 cm. The bioturbation caused by the brittle stars may change the physical properties of the sediments, as reported by Rowden et al. (1998). They found that the shear strength of the upper 5 cm of sediment was reduced by up to 45% due to bioturbation. This also may influence the acoustic properties of sediments, like firmness.

A. filiformis can switch between two different feeding types. For deposit feeding, the arm tips explore the sediment surface for particles. For suspension feeding, the arms are held vertically to 2–4 cm above the sediment surface to trap particulate suspended matter and phytoplankton (Buchanan 1964; Woodley 1975; Loo et al. 1996). The number of active feeding arms seems to vary. Ockelmann and Muus (1978) described 3–4 active arms per individual, whereas Loo et al. (1996) and Rosenberg et al. (1997) observed only 1–2. In the present study, the mean abundance of brittle stars/m^2 in community C would result in a minimum of 1,711 arms/m^2 (cf. one active arm per individual) and a maximum of 6,844 arms/m^2 (cf. four active arms). Since most of the specimens were adults, the mean length of the arms above the sediment surface probably reached 5–6 cm.

The high number of ophiuroid arms inferred for the subarea of the present study is expected to influence the surface roughness of the seafloor, causing a change in backscattering (cf. Lurton 2002). The roughness data (E1) from RoxAnn (Fig. 4) show higher values in the southern part of the subarea. This indicates that the high number of ophiuroid arms increased the roughness of the seafloor. Such changes in surface micro-roughness can influence the backscattering signal and acoustic classification (Bartholomä et al. 2011). Capperucci and Bartholomä (2012) confirmed that, for high-frequency hydroacoustic systems (>100 kHz), such roughness changes may influence the acoustic signals more than actual changes of sediment composition. It is also important to note that the seafloor classes are based on the acoustic response of the footprint of the sonar system from both the seafloor itself and the arms of the ophiuroids. For a single-beam echosounder, the seafloor footprint size is based on water depth. At a water depth of 30 m, the QTC 5.5 system ensonifies an area of 11.8 m^2. Thus, the seafloor classification pattern of the southern part of the subarea of the present study would be influenced by changes in seafloor roughness and hardness caused by thousands of feeding arms of the brittle star A. filiformis.

Conclusions

Acoustic seafloor mapping and automatic classification is in general a valuable tool for the study of sediment distribution and also the EU MSFD descriptor "seafloor integrity". In order to obtain reliable results, it is suggested to run at least two different systems simultaneously during a survey. One of these should be a swath system like a dual-frequency sidescan sonar or multi-beam echosounder. The other should be a single-beam echosounder-based acoustic seafloor classification system working in the 200 kHz range. The different grazing angles (high for single-beam systems and medium to low for sidescan sonar, and medium to high for multi-beam echosounder systems) reduce the effects of volume backscattering and surface roughness. A thorough ground-truthing program is required. Based on the similarities of classifications, the best choice for habitats like the northwest Helgoland area would be a sidescan sonar and the RoxAnn seafloor classification system.

Sidescan sonar data showed a slight increase of backscatter strength from the northeast to the southwest in the subarea chosen for more detailed surveying in the present study. Automatic seafloor classification methods segmented the area of increased backscatter intensity in the southern sector of the subarea as separate class, although the sediment texture was not significantly different from that in the north-western sector (muddy fine sand to muddy very fine sand). The abundance of molluscs decreases from the north to the south of the subarea, whereas that of Echinodermata increases (especially *A. filiformis*). The correlation between the abundance of *A. filiformis* feeding arms and backscatter intensity in the southern sector revealed that most likely the feeding arms increased the sediment surface roughness and, thus, the backscatter intensity. It is suggested that the *A. filiformis* community C covers large parts of the subarea. The number of grab samples for macrofauna studies can be reduced significantly by the use of hydroacoustic data and automatic seafloor classification, saving time and money. The seafloor sediment distribution from acoustic backscatter and automatic seafloor classification shows a much higher resolution than from extrapolation of surface samples alone.

Compliance with ethical standards

Conflict of interest The authors declare that there is no conflict of interest with third parties.

References

Anderson JT, Van Holliday D, Kloser R, Reid DC, Simard Y (2008) Acoustic seabed classification: current practice and future directions. ICES J Mar Sci 65:1004–1011

Bartholomä A (2006) Acoustic bottom detection and seabed classification in the German Bight, southern North Sea. Geo-Mar Lett 26: 177–184

Bartholomä A, Holler P, Schrottke K, Kubicki A (2011) Acoustic habitat mapping in the German Wadden Sea - comparison of hydroacoustic devices. J Coast Res SI 64:1–5

Bornhold BD, Collins WT, Yamanaka L (1999) Comparison of seabed characterization using sidescan sonar and acoustic classification techniques. In: Proc Canadian Coastal Conf, Victoria, Canada, 15 pp

Bray JR, Curtis JT (1957) An ordination of the upland forest communities of southern Wisconsin. Ecol Monogr 27:325–349

Brown CJ, Collier JS (2008) Mapping benthic habitat in regions of gradational substrata: an automated approach utilising geophysical, geological, and biological relationships. Estuar Coast Shelf Sci 78:203–214

Brown CJ, Mitchell A, Limpenny DS, Robertson MR, Service M, Golding N (2005) Mapping seabed habitats in the Firth of Lorn off the west coast of Scotland: evaluation and comparison of habitat maps produced using the acoustic ground-discrimination system. RoxAnn, and sidescan sonar. ICES J Mar Sci 62:790–802

BSH (2016) Guideline for seafloor mapping in German marine waters using high resolution sonars. BSH no 7201. Bundesamt für Seeschifffahrt und Hydrographie, Hamburg, Germany

Buchanan JB (1964) A comparative study of some features of the biology of *Amphiura filiformis* and *Amphiura chiajei* (Ophiuroidea) considered in relation to their distribution. J Mar Biol Assoc UK 44:565–576

Cadée CC (1984) Macrobenthos and macrobenthic remains in the Oyster Ground, North Sea. Neth J Sea Res 18:160–178

Capperucci RM, Bartholomä A (2012) Sediment vs topographic roughness: anthropogenic effects on acoustic seabed classification. In: Proc Hydro 2012, Rotterdam, p 47–52

Chivers RC, Emerson NC, Burns D (1990) New acoustic processing for underway surveying. Hydrogr J 56:9–17

Clarke KR, Gorley RN (2006) PRIMER v6: user manual/tutorial. PRIMER-E, Plymouth

Clarke KR, Green RH (1988) Statistical design and analysis for a "biological effects" study. Mar Ecol Prog Ser 46:213–226

Clarke KR, Warwick RM (2001) Change in marine communities: an approach to statistical analysis and interpretation, 2nd edn. PRIMER-E, Plymouth

Collins WT, Galloway JL (1998) Seabed classification and multibeam bathymetry: tool for multidisciplinary mapping. Sea Technol 39:45–49

Dean BJ, Ellis JT, Irlandi (2013) Measuring nearshore variability in benthic environments: an acoustic approach. Ocean Coast Manag 86:3–41

Degraer S, Moerkerke G, Rabaut M, Van Hoey G, Du Four I, Vincx M, Henriet J-P, Van Lancker V (2008) Very-high resolution side-scan sonar mapping of biogenic reefs of the tube-worm *Lanice conchilega*. Remote Sens Environ 112:3323–3328

European Union (2008) Directive 2008/56/EC of the European Parliament and of the Council of 17 June 2008 establishing a framework for community action in the field of marine environmental

policy (Marine Framework Directive). In: Official Journal of the European Union, vol L164, p 19–40

Ferrini VL, Flood RD (2006) The effects of fine-scale surface roughness and grain size on 300 kHz multibeam backscatter intensity in sandy marine sedimentary environments. Mar Geol 228:153–172

Figge K (1981) Karte zur Sedimentverteilung in der Deutschen Bucht, Nr. 2900. Bundesamt für Seeschifffahrt und Hydrographie, Hamburg, Germany, scale 1:250,000

Flemming BW, Thum A (1978) The settling tube - a hydraulic method of grain size analysis of sands. Kiel Meeresforsch SI 4:82–95

Folk RL (1954) The distinction between grain size and mineral composition in sedimentary rock nomenclature. J Geol 62(4):344–359

Freitas R, Ricardo F, Pereira F, Sampaio L, Carvalho S, Gaspar M, Quintino V, Rodrigues AM (2011) Benthic habitat mapping: concerns using a combined approach (acoustic, sediment and biological data). Estuar Coast Shelf Sci 92:598–606

Gleason ACR (2009) Single-beam acoustic seabed classification in coral reef environments with application to the assessment of grouper and snapper habitat in the upper Florida Keys, USA. PhD Thesis, University of Miami, Coral Gables, FL

Gleason ACR, Eklund AM, Reid RP, Koch V (2006) Acoustic seabed classification, acoustic variability, and grouper abundance in a forereef environment. NOAA Prof Papers NMFS 5, p 38–47

Hammer Ø, Harper DAT, Ryan PD (2001) PAST: paleontological statistics software package for education and data analysis. Palaeontol Electron 4(1):1–9

Hartmann-Schröder G (1996) Teil 58. Annelida, Borstenwürmer, Polychaeta. 2. neubearb. Auflage. In: Dahl F, Schuhmann H (eds) Die Tierwelt Deutschlands und der angrenzenden Meeresteile nach ihren Merkmalen und nach ihrer Lebensweise. Zoologisches Museum Berlin, Jena

Hass HC, Bartsch I (2008) Acoustic kelp bed mapping in shallow rocky coasts - case study Helgoland. In: Doerffer R, Colijn F, van Beusekom J (eds) Observing the coastal sea - an Atlas of advanced monitoring techniques. LOICS Reports & Studies, no 33. GKSS Research Centre, Geesthacht, Germany, p 50–53

Hass HC, Mielck F, Fiorentino D, Papenmeier S, Holler P, Bartholomä A (2016) Seafloor monitoring west of Helgoland (German Bight, North Sea) using the acoustic ground discrimination system RoxAnn. Geo-Mar Lett. doi:10.1007/s00367-016-0483-1

Huff LC (2008) Acoustic remote sensing as a tool for habitat mapping in Alaska waters. In: Reynolds JR, Greene HG (eds) Marine habitat mapping technology for Alaska. Alaska Sea Grant College Program, University of Alaska Fairbanks. doi:10.4027/mhmta.2008.03

Josefson AB (1998) Resource limitation in marine soft sediments - differential effects of food and space in the association between the brittle-star *Amphiura filiformis* and the bivalve *Mysella bidentata*. Hydrobiologia 375(376):297–305

Kenny AJ, Cato I, Desprez M, Fader G, Schüttenhelm RTE, Side J (2003) An overview of seabed-mapping technologies in the context of marine habitat classification. ICES J Mar Sci 60:411–418

Kröncke I, Stoeck T, Wieking G, Palojärvi A (2004) Relationship between structural and functional aspects of microbial and macrofaunal communities in different areas of the North Sea. Mar Ecol Prog Ser 282:13–21

Kröncke I, Reiss H, Eggleton JD, Aldridge J, Bergman MJN, Cochrane S, Craeymeersch J, Degraer S, Desroy N, Dewarumez J-M, Duineveld G, Essink K, Hillewaert H, Lavaleye MSS, Moll A, Nehring S, Newell J, Oug E, Pohlmann T, Rachor E, Robertson M, Rumohr H, Schratzberger M, Smith R, Vanden Berghe E, van Dalfsen J, van Hoey G, Vincx M, Willems W, Rees HL (2011) Changes in North Sea macrofauna communities and species distribution between 1986 and 2000. Estuar Coast Shelf Sci 94:1–15

Krumbein WC, Aberdeen E (1937) The sediments of Barataria Bay. J Sediment Petrol 7:3–17

Kühne S, Rachor E (1996) The macrofauna of a stony sand area in the German Bight (North Sea). Helgoländer Meeresun 50:433–452

Künitzer A (1989) Factors affecting the population dynamics of *Amphiura filiformis* (Echinodermata: Ophiuroidea) and *Mysella bidentata* (Bivalvia: Galeommatacea) in the North Sea. In: Ryland JS, Tyler PA (eds) Reproduction, genetics and distributions of marine organisms. Proc 23rd Europ Mar Biol Symp. Olsen & Olsen, Fredensborg, Denmark, p 395–406

Künitzer A, Basford D, Craeymeersch JA, Dewarumez JM, Dörjes J, Duinveld GCA, Eleftheriou A, Heip C, Herman P, Kingston P, Niermann U, Rachor E, Ruhmor H, de Wilde PAJ (1992) The benthic infauna of the North Sea: species distribution and assemblages. ICES J Mar Sci 49:127–143

Loo L-O, Jonsson PR, Sköld M, Karlsson Ö (1996) Passive suspension feeding in *Amphiura filiformis* (Echinodermata: Ophiuroidea): feeding behaviour in flume flow and potential feeding rate of field populations. Mar Ecol Prog Ser 139:143–155

Lucieer V (2008) Object-oriented classification of sidescan sonar data for mapping benthic marine habitats. Int J Mar Sensing 29:905–921

Lurton X (2002) An introduction to underwater acoustics: principles and applications. Springer, London

Lurton X, Lamarche G (eds) (2015) Backscatter measurements by seafloor-mapping sonars. Guidelines and recommendations. http://geohab.org/wp-content/uploads/2014/05/BSWG-REPORT-MAY2015.pdf

Markert E, Holler P, Kröncke I, Bartholomä A (2013) Benthic habitat mapping of sorted bedforms using hydroacoustic and ground-truthing methods in a coastal area of the German Bight/North Sea. Estuar Coast Shelf Sci 129:94–104

Mazel C (1985) Side scan sonar record interpretation. Klein Associates Inc, Report 11230001 Rev 01

Micallef A, Le Bas TP, Huvenne VAI, Blondel P, Hühnerbach V (2012) A multi-method approach for benthic habitat mapping of shallow coastal areas with high-resolution multibeam data. Cont Shelf Res 39(40):14–26. doi:10.1016/j.csr.2012.03.008

Mielck F, Bartsch I, Hass HC, Wölfl A-C, Bürk D, Betzler C (2014) Predicting spatial kelp abundance in shallow coastal waters using the acoustic ground discrimination system RoxAnn. Estuar Coast Shelf Sci 143:1–11

Ockelmann KW, Muus K (1978) The biology, ecology and behaviour of the bivalve *Mysella bidentata* (Montagu). Ophelia 17:1–93

Pielou E (1969) An introduction to mathematical ecology. Wiley, New York

Preston JM (2006) Acoustic classification of seaweed and sediment with depth-compensated vertical echoes. In: Proc MTS/IEEE Oceans 2006 Conf, Boston, USA, p 1–5

Preston JM, Parrott DR, Collins WT (2003) Sediment classification based on repetitive multibeam bathymetry surveys of an offshore disposal site. In: Proc IEEE Oceans '03 Conf, p 69–75

Preston JM, Christney AC, Beran LS, Collins WT (2004) Statistical seabed segmentation - From images and echoes to objective clustering. In: Proc 7th European Conf Underwater Acoustics, Delft, The Netherlands, p 813–813

Quester Tangent Corporation (2003) Mapping intertidal oysters with QTC View, North Inlet-Winyah Bay, South Carolina. QTC Technical Report SR41-03

Quester Tangent Corporation (2011) QTC Swathview 11.1. User manual and reference: DMN-SWVV-0000-R02

Rachor E, Nehmer P (2003) Erfassung und Bewertung ökologisch wertvoller Lebensräume in der Nordsee. Abschlussbericht F+E, Vorhaben FKZ 89985310, Bundesamt für Naturschutz

Reiss H, Meybohm K, Kröncke I (2006) Cold winter effects on benthic macrofauna communities in near-and offshore regions of the North Sea. Helgol Mar Res 60:224–238

Rice J, Arvanitidis C, Borja A, Frid C, Hiddink JG, Krause J, Lorance P, Ragnarsson SA, Sköld M, Trabucco B, Enserink L, Norkko A

(2012) Indicators for sea-floor integrity under the European Marine Strategy Framework Directive. Ecol Indic 12:174–184

Riegl BM, Halfar J, Purkis SJ, Godinez-Orta L (2007) Sedimentary facies of the eastern Pacific's northernmost reef-like setting (Cabo Pulmo, Mexico). Mar Geol 236:61–77

Rosenberg R, Nilsson HC, Hollertz K, Hellman B (1997) Density-dependent migration in an *Amphiura filiformis* (Amphiuridae, Echinodermata) infaunal population. Mar Ecol Prog Ser 159: 121–131

Rowden AA, Jago CF, Jones SE (1998) Influence of benthic macrofauna on the geotechnical and geophysical properties of surficial sediments, North Sea. Cont Shelf Res 18:1347–1362

Salzwedel H, Rachor E, Gerdes D (1985) Benthic macrofauna communities in the German Bight. Veröff Inst Meeresforsch Bremerh 20: 199–267

Schimel ACG, Healy TR, McComb P, Immenga D (2010a) Comparison of a self-processed EM3000 multibeam echosounder dataset with a QTC View habitat mapping and a sidescan sonar imagery, Tamaki Strait, New Zealand. J Coast Res 26(4):714–725

Schimel ACG, Healy TR, Johnson D, Immenga D (2010b) Quantitative experimental comparison of single-beam, sidescan, and multibeam benthic habitat maps. ICES J Mar Sci 67:1766–1779

Schlagintweit GEO (1993) Real-time acoustic bottom classification for hydrography: a field evaluation of RoxAnn. Canadian Hydrographic Services, Department of Fisheries and Oceans, Canada

Shannon CE, Weaver W (1949) The mathematical theory of communication. University of Illinois Press, Urbana

Sköld M, Loo L-O, Rosenberg R (1994) Production, dynamics and demography of an *Amphiura filiformis* population. Mar Ecol Prog Ser 103:81–90

Southward EC, Campbell AC (2006) Echinoderms: Keys and notes for the identification of British species. Synopses of the British fauna (New Series), no 56. Field Studies Council, Shrewsbury

Spaeth C (1990) Zur Geologie der Insel Helgoland. Die Küste 49:1–32

Spearman CE (1904) The proof and measurement of association between two things. Am J Psychol 15:72–101

Stein R (1985) Rapid grain-size analyses of clay and silt fractions by SediGraph 5000d: comparison with Coulter Counter and Atterberg methods. J Sediment Petrol 55(4):590–593

Tucker M (1988) Techniques in sedimentology. Blackwell, Oxford

van Overmeeren R, Craeymeersch J, van Dalfsen J, Fey F, van Heteren SM, van Meesters E (2009) Acoustic habitat and shellfish mapping and monitoring in shallow coastal water – sidescan sonar experiences in the Netherlands. Estuar Coast Shelf Sci 85(3):437–448

Verfaillie E, Doornebal P, Mitchell AJ, White J, Van Lancker V (2007) The bathymetric position index (BPI) as a support tool for habitat mapping. Worked example for the MESH Final Guidance. www.searchmesh.net

Wentworth CK (1922) A scale of grade and class terms for clastic sediments. J Geol 30:377–392

Wienberg C, Bartholomä A (2005) Acoustic seabed classification of a coastal environment (outer Weser Estuary – German Bight) - a new approach to monitor dredging and dredge spoil disposal. Cont Shelf Res 25:1143–1156

Winter C, Herrling G, Bartholomä A, Capperucci R, Callies U, Heipke C, Schmidt A, Hillebrand H, Reimers C, Bremer P, Weiler R (2014) Scientific concepts for monitoring the ecological state of German coastal seas (in German). Wasser und Abfall 2014:21–26. doi:10.1365/s35152-014-0685-7

Woodley JD (1975) The behaviour of some amphiuroid brittle-stars. J Exp Mar Biol Ecol 18:29–46

Wright DJ, Lundblad ER, Larkin EM, Rinehart RW, Murphy J, Cary-Cothera L, Draganov K (2005) ArcGIS Benthic Terrain Modeler. Oregon State University, Corvallis, Davy Jones Locker Seafloor Mapping/Marine GIS Laboratory and NOAA Coastal Services Center. http://www.csc.noaa.gov/digitalcoast/tools/btm